Low Temperature Physics/Fizika Nizkikh Temperatur, 2020, v. 46, No. 4, pp. 416–421

Physics of vortex motion by means of microwave surface impedance measurements

(Review article)

N. Pompeo, A. Alimenti, K. Torokhtii, and E. Silva

Dipartimento di Ingegneria, Università Roma Tre, Via Vito Volterra 62, Roma 00146, Italy
E-mail: nicola.pompeo@uniroma3.it

Received December 5, 2019, published online February 28, 2020

In this paper we present a short overview on the results that can be obtained through the study of vortex motion at high frequencies. The phenomenological force balance for isolated-like vortices shaken by microwave currents and subjected to viscous drag, pinning forces and thermal creep is recalled and physically presented. The derived vortex motion resistivity, together with the main vortex parameters (viscosity η and flux flow resistivity ρ_{ff}, pinning constant k_p, creep factor χ), is then commented. Sample measurements are reported to illustrate the main aspects of the involved physical models.

Keywords: surface impedance, flux flow resistivity, pinning constant.

Contents

1. Introduction

High frequency studies of the electrodynamic response of superconductors in the microwave range (1–100 GHz) were fundamental for the understanding of their physics, allowing for the determination, among the others [1], of the existence [2] and type [3] of superconducting gap, of the penetration depth [4], of critical fields [5], of dynamical fluctuations [6], of the material anisotropy [7] and of pinning anisotropy [8]. Studies of type II superconductors in the mixed state are also relevant in view of applications. For example, a revamped interest has recently emerged in frontier fields like the hunt for Cold Dark Matter and detection of axions [9,10] or particle physics with the design of future colliders [11], where superconductors are required to work in high magnetic fields. Other recent lines of research worth mentioning deal with the study of microwave-stimulated superconductivity in the mixed state [12,13]; of superconductor/ferromagnet multilayers, where, e.g., anomalous flux flow [14,15], magnon-fluxon interaction [16] and thermodynamic 0–π transition [17] were observed and tunable motion of vortices through the rotation of magnetic moments implemented [18]; of the imaging of high-speed vortices [19] and the exploitation of their motion for electromagnetic emission at microwaves [20]. In this paper we will first focus on the models and concepts of the high-frequency vortex dynamics (Sec. 2), then we will present example experimental results on selected topics (Sec. 3), concluding with a few remarks.

2. High-frequency electrodynamic response in superconductors in the mixed state

In the microwave frequency range, the relevant experimental quantity describing the frequency $f = \omega/(2\pi)$ dependent electrodynamic response of a (super)conductor is the so-called *surface impedance* Z_s [21]:

$$Z_s \equiv \frac{E_{||}}{H_{||}} = R_s + iX_s, \tag{1}$$

where $E_{||}$ and $H_{||}$ are the components of the electric and magnetic fields tangential to the material limiting surface, and R_s and X_s are the surface resistance and reactance. The surface impedance can be measured with various

techniques and methods, with resonant methods preferred because of their sensitivity (for a review, see e.g. [22,23]).

The explicit link between Z_s and the relevant material property, the conductivity σ (or the resistivity ρ), depends on the sample geometry and on the actual electromagnetic (e.m.) field configuration. The bulk regime is prototypical: there, the sample thickness $t_s \gg (\lambda, \delta_n)$, i.e. much larger than the length scale of exponential attenuation of the penetrating e.m. field (being λ and δ_n the London penetration and normal skin depth, respectively). One then finds $Z_s = \sqrt{i\omega\mu_0\rho}$ in the local limit. For arbitrary t_s, the relation $Z_s \leftrightarrow \rho$ can be considerably more intricate [24–26], with possible simplifications in thin films [27] where the approximation $Z_s \simeq \rho/t_s$ can be sometimes exploited.

The conductivity σ in the high-frequency regime, in zero magnetic field, is customarily described by the two-fluid model [28] $\sigma_{2f} = \sigma_1 - i\sigma_2 = \sigma_{QP} - i/(\omega\mu_0\lambda^2)$, with parallel conduction channels attributed to superfluid σ_2 (purely inductive, with λ the London penetration depth) and to quasi-particle "normal" excitations σ_{QP}.

The application of a magnetic field larger than the lower critical field H_{c1} drives a type II superconductor in the mixed state. For $H > H_{c1}$ fluxons (or "vortices") thread the superconductor and experience a Lorentz force (more generally, a Magnus force, see e.g. [29,30] for a discussion of the nature of the force involved) by the microwave currents which set them in oscillatory motion around their equilibrium positions. Fluxon motion, in turn, induces a varying electric field which couples back with the currents. This interplay has been addressed by various authors [31,32]; self-consistently solving for the e.m. and current distribution and vortex motion for small displacements $\mathbf{u}$ [31] yields an overall resistivity $\tilde{\rho}$ that can be written down as:

$$\tilde{\rho} = \frac{\rho_{vm} + i/\sigma_2}{1 + i\sigma_1/\sigma_2}, \tag{2}$$

where ρ_{vm} is the so-called vortex motion resistivity [33,34].

In order to derive an explicit expression for ρ_{vm}, one writes down a single-vortex equation for the balance of the forces (per unit length). The single-vortex dynamics is justified by the small oscillation amplitudes, smaller than the intervortex spacing. In addition, one assumes that vortices experience the same pinning potential. Thus, the following phenomenological force (per unit length) balance equation for a single fluxon (with flux quantum Φ_0 and axis along the field direction $\hat{\mathbf{n}}$) moving with speed $\mathbf{v}$ is written down

$$\eta\mathbf{v} + k_p\mathbf{u} = \mathbf{J} \times (\hat{\mathbf{n}}\Phi_0) + \mathbf{F}_{\text{therm}}, \tag{3}$$

which describes the vortex as a massless damped harmonic forced oscillator, additionally subjected to a force representing thermal forces. For simplicity's sake, no Hall terms have been considered here [30,34]; similarly, no vortex mass term (of the order of the total mass of the electrons in the vortex core [30]) has been included, since it can be relevant only at the high edge of the microwave frequency region [30].

From Eq. (3) ρ_{vm} is derived as

$$\rho_{vm} = \rho_{ff}\frac{\chi + i\omega/\omega_0}{1 + i\omega/\omega_0}, \tag{4}$$

which contains the flux flow resistivity $\rho_{ff} = \Phi_0 B/\eta$ as a prefactor and a characteristic angular frequency ω_0 related to pinning. Each parameter in Eqs. (3) and (4) represents a peculiar aspect of the physics of the vortex motion, which we now describe.

Viscosity — flux flow resistivity: the viscous drag force $-\eta\mathbf{v}$, with *viscosity* η, or equivalently ρ_{ff}, accounts for power dissipation due to non-equilibrium conversions between QP and condensate [28] during the motion of vortices. Microscopically, $\eta \propto \langle\omega_c\tau\rangle_F$ [34] where ω_c is the cyclotron angular frequency at B_{c2}, τ is the QP scattering time in the vortex cores and $\langle\rangle_F$ represents the average over the Fermi surface [35]. Thus, η yields information about QP scattering time and density of states in vortex cores [28,36] and also outside for nodal superconductors [37]. Through η or ρ_{ff} different scattering regimes (dirty, clean, superclean) and scattering impurities can be identified [38–40], together with signatures for nodal/multiple superconducting gaps [35,39,41]. It is worth stressing here that in ac measurements, even in presence of pinning which in dc prevents the exploration of the free flux flow regime, the simultaneous determination of the real and imaginary parts of the complex ρ_{vm} allows for the extraction of ρ_{ff}.

Pinning constant: the elastic recall force $-k_p\mathbf{u}$ is due to pinning: material defects with lowered condensation energy density allow to lower the overall system energy when occupied by fluxons, thus becoming preferential sites for fluxons. Describing their action as a spatially varying pinning potential, the displacement $\mathbf{u}$ of fluxons from the equilibrium sites (i.e the bottom of the pinning wells) is contrasted by a pinning recall force. The latter, for the small displacements occurring at high (microwave) frequencies, can be linearized in $\mathbf{u}$, with k_p the so-called pinning constant or Labusch parameter [42]. A rough estimation of the maximum value $k_p^{\max} \sim \mu_0 H_c^2$ for core pinning of "rigid" fluxons due to a defect having size equal to the fluxon can be obtained equating the maximum "spring" pinning energy $1/2 k_p^{\max}\xi^2$ (being ξ the coherence length) with the lost condensation energy per unit length of the vortex $1/2\mu_0 H_c^2$ (where H_c is the thermodynamic critical field) having cross-area $\propto \xi^2$ [34]. In this limiting situation ("single vortex pinning") k_p is independent from B (being $B = \mu_0 H$, in the London limit).

More generally, the effects of finite vortex line tension, of heterogeneous pins, of collective pinning [34,39,43] can be to some extent included considering an effective field dependent $k_p(H)$.

Thermal creep: to take quantitatively into account the thermal effects on vortex motion, one assumes a Langevin expression for the thermal force $\mathbf{F}_{\text{therm}}$. In Eq. (4) the *creep parameter* χ then appears, with $0 \le \chi \le 1$. In the zero creep $\chi = 0$ limiting case, the characteristic frequency $\omega_0 \to \omega_p = k_p/\eta$, the well-known (de)pinning angular frequency [44], first introduced in the seminal Gittleman–Rosenblum work [33], which separates the low frequency, low dissipation elastic dominated regime ($\omega \ll \omega_p$) from the high frequency, high dissipation regime ($\omega \gg \omega_p$). In the opposite limit of maximum creep $\chi = 1$, thermally activated jumps completely wash out the pinning potential leaving only a pure flux flow.

Anisotropy: lastly, it has to be noted that the above scalar equations have been written considering isotropic superconductors. Moreover, the Lorentz force — when $\mathbf{J} \not\perp \mathbf{B}$, material anisotropy, and excitation microwave current with different orientations on the sample surface (as typical in many experimental setups [22]), can yield generally $\mathbf{J} \not\parallel \mathbf{E}$, so that a tensor description, with its added complexity, is mandatory. Finally, pinning centers with different dimensionalities (point, linear, planar or particles) bring an additional angular dependence, which is actively studied and investigated to optimize technologically relevant superconductors [45]. A tensorial treatment of the vortex dynamics which enables to address these scenarios is reported in [46,47].

Frequency dependence: more complex dynamics appear when the vortex oscillation time becomes comparable with the fluxon system propagation times of the perturbation (e.g. in the frequency range of tens of MHz [48]), or when more than one collective oscillatory mode takes place (e.g. due to concurrent surface and volume pinning [49]) or when the fluxon system is near a liquid-glass transition (below 1 GHz, as determined in YBCO [50]). In these cases, the simple Eq. (3) with its single zero/pole frequency dependence fails and more complex models are required [39,48,51].

3. Measurement examples

In this Section we present some sample measurements, performed at fixed frequency and temperature T by means of a dielectric resonator operating at $f = 47.3$ GHz [52], which exemplifies the typical information that can be gained from a high-frequency study. Samples are cuprate thin (100–200 nm) films: pure $YBa_2Cu_3O_{7-\delta}$ (YBCO), YBCO added with $BaZrO_3$–based artificial pinning centers (YBCO/BZO) to increase pinning efficacy, and $Tl_2Ba_2CaCu_2O_{8+x}$ (TBCCO). First presented measurements are performed by applying a varying magnetic field ($0 < \mu_0 H < 0.8\,T$) perpendicular to the sample surfaces, i.e. parallel to the material crystallographic c axis. The induced variations of the surface impedance $\Delta Z_s(H) = Z_s(H) - Z_s(0) \simeq \rho_{vm}(H)/d$ was measured at fixed $T = 76$–77 K, yielding directly $\rho_{vm} \simeq \tilde{\rho}$ since σ_{2f} is essentially field-independent at low H. Neglecting creep (see [53] for the evaluation of the corresponding uncertainties arising through this approach), the flux flow resistivity ρ_{ff} (Fig. 1, in YBCO for various T; Fig. 2, in the various materials at fixed T) and the pinning constant $k_p(H)$ (Fig. 3) are extracted through Eq. (4). It can be seen that $\rho_{ff}(H)$ vs H in YBCO is almost linear, and increases with T, consistently with a constant η, as foreseen by simpler models at low fields [54], according to which $\rho_{ff} = \rho_n B/B_{c2}$ (with ρ_n the normal state resistivity). In Fig. 2, it can be seen that the addition of BZO particles does not significantly change ρ_{ff}. On the other hand, the flux flow resistivity in TBCCO exhibits larger values even if the reduced temperature is lower ($T_c \sim 92$ K and $T_c \sim 104$ K for the presented YBCO and TBCCO samples, respectively). The cause of this large difference (almost one order of magnitude) is to be ascribed to the fundamental physics of the quasi-particles dissipation in the vortex cores, since $\rho_{ff} \propto \eta^{-1} \propto \langle \omega_c \tau \rangle_F^{-1}$ (see Sec. 2). Concerning pinning (see Fig. 3), it can be seen that BZO-addition increases the pinning effectiveness, yielding k_p with higher values in YBCO/BZO with respect to YBCO; TBCCO, on the other hand, exhibits the lowest values, even if the reduced temperature T/T_c is lower. Also the field dependence changes: almost constant in YBCO/BZO,

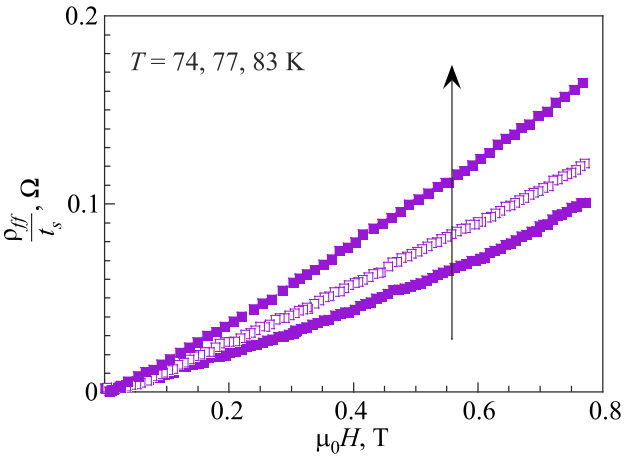

Fig. 1. $\rho_{ff}(H)$ for selected T in a YBCO sample.

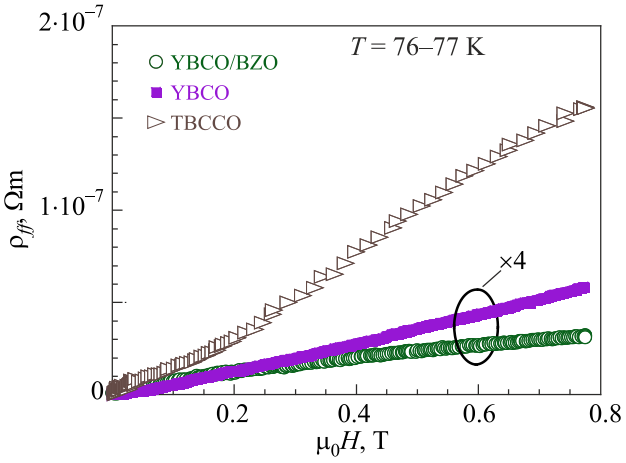

Fig. 2. $\rho_{ff}(H)$ in various cuprate samples.

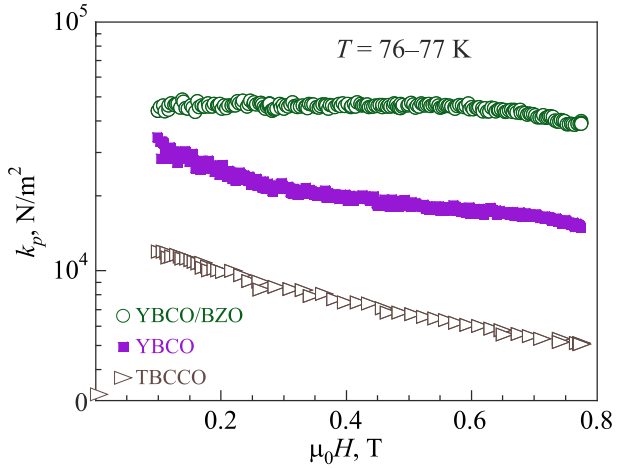

Fig. 3. $k_p(H)$ in various cuprate samples.

hinting to more rigidly pinned and short-moving fluxons, down to TBCCO which exhibits a pronounced decreasing k_p, linked to its softer flux lines caused by higher anisotropy [39].

Figure 4 presents angular measurements performed on a YBCO thin film at $T = 78$ K. By varying the angle θ between the magnetic field $\mathbf{H_0}$ with fixed intensity $H_0 = 0.75$ T and the sample c axis, $\rho_{vm}(\theta)$ was obtained. Through the analysis described in [55], a mass anisotropy $\gamma = 5$ was determined, and hence, the $k_p(\theta)$. It can be seen that $k_p(\theta)$ shows a feature-rich angular dependence which allows to discriminate the superposition of the mass anisotropy (wide hump) and ab planes pinning (tight peak around $\theta = 90^\circ$).

4. Final remarks

In this short review we have presented some of the physics which can be extracted from high-frequency electrodynamic studies of superconductors in the mixed state.

We have shown that a lot of important information can be extracted: measuring the real and imaginary parts of the resistivity allows for the extraction of the flux-flow resistivity from the pinning effects. We have shown that the flux-flow resistivity in YBCO exhibits a conventional, linear dependence with the applied field. The pinning constant is very material dependent. In particular, k_p reaches large values in YBCO with BZO nanorods. Moreover, the field dependence in the YBCO/BZO sample is mainly flat, pointing to the promotion of a single-pinning regime. By contrast, in TBCCO k_p attains its lowest values, because of the very large anisotropy of TBCCO. We should mention that we have limited ourselves to linear regimes with respect the excitation currents power levels. When the microwave power is high enough, important nonlinear effects set in [56,57]. Applications such as beam screen for the future colliders in the high energy physics, where one expects high power levels in the GHz range in intense magnetic fields (of the order of 16 T) [11], present challenging scenarios which open new research line to be investigated.

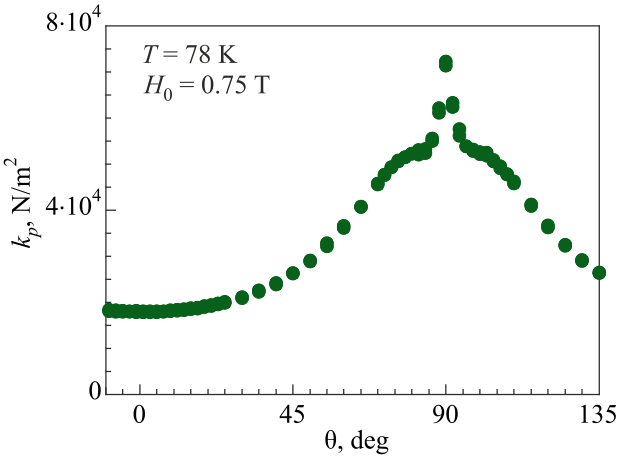

Fig. 4. $k_p(\theta)$ in a YBCO sample.

Acknowledgments

This work has been partially carried out within the framework of the EUROfusion Consortium and has received funding from the Euratom Research and Training Programme 2014-2018 and 2019-2020 under grant agreement No 633053. The views and opinions expressed herein do not necessarily reflect those of the European Commission. The authors warmly thank V. Pinto, A. Augieri, G. Celentano and the Superconductivity Division of ENEA, Frascati, Italy for having provided the YBCO samples; H. Schneidewind of the Leibniz Institute of Photonic Technology, Jena, Germany, for having provided the TBCCO sample.

1. A. Maeda, H. Kitano, and R. Inoue, *J. Phys. Condens. Matter* **17**, R143 (2005).
2. M. Biondi, A. Forrester, M. Garfunkel, and C. Satterthwaite, *Rev. Mod. Phys*. **30**, 1109 (1958).
3. W.N. Hardy, D.A. Bonn, D.C. Morgan, R. Liang, and K. Zhang, *Phys. Rev. Lett*. **70**, 3999 (1993).
4. J.R. Waldram, *Adv. Phys*. **13**, 1 (1964).
5. B. Rosenblum and M. Cardona, *Phys. Rev. Lett*. **12**, 657 (1964).
6. R. D'Aiello and S. Freedman, *Phys. Rev. Lett*. **22**, 515 (1969).
7. E. Bartolomé, F. Vallés, A. Palau, V. Rouco, N. Pompeo *et al.*, *Phys. Rev. B* **100**, 054502 (2019).
8. N. Pompeo, A. Alimenti, K. Torokhtii, E. Bartolome, A. Palau *et al.*, *Supercond. Sci. Technol*. (2020), in press.
9. D. Alesini, C. Braggio, G. Carugno, N. Crescini, D.D. Agostino *et al.*, *Phys. Rev. D* **99**, 101101 (2019).
10. D. Di Gioacchino, C. Gatti, D. Alesini, C. Ligi, S. Tocci *et al.*, *IEEE Trans. Appl. Supercond*. **29**, 3500605 (2019).

11. A. Abada, M. Abbrescia, S.S. AbdusSalam, I. Abdyukhanov, J.A. Fernandez *et al*., *Eur. Phys. J. Spec. Top*. **228**, 755 (2019).
12. A. Lara, F.G. Aliev, A.V. Silhanek, and V.V. Moshchalkov, *Sci. Rep*. **5**, 9187 (2015).
13. O.V. Dobrovolskiy, R. Sachser, V.M. Bevz, A. Lara, F.G. Aliev *et al*., *Phys. Status Solidi (RRL)* **13**, 1800223 (2019).
14. K. Torokhtii, N. Pompeo, C. Meneghini, C. Attanasio, C. Cirillo *et al*., *J. Supercond. Nov. Magn*. **26**, 571 (2012).
15. A. Vargunin and M. Silaev, *Sci. Rep*. **9**, 5914 (2019).
16. O.V. Dobrovolskiy, R. Sachser, T. Brächer, T. Böttcher, V. V. Kruglyak *et al*., *Nat. Phys*. **15**, 477 (2019).
17. N. Pompeo, K. Torokhtii, C. Cirillo, A.V. Samokhvalov, E.A. Ilyina *et al*., *Phys. Rev. B* **90**, 064510 (2014).
18. V.K. Vlasko-Vlasov, F. Colauto, T. Benseman, D. Rosenmann, and W.-K. Kwok, *Sci. Rep*. **6**, 36847 (2016).
19. L. Embon, Y. Anahory, Ž.L. Jelić, E.O. Lachman, Y. Myasoedov *et al*., *Nat. Commun*. **8**, 85 (2017).
20. O.V. Dobrovolskiy, V.M. Bevz, M.Y. Mikhailov, O.I. Yuzephovich, V.A. Shklovskij *et al*., *Nat. Commun*. **9**, 4927 (2018).
21. R.E. Collin, *Foundations for microwave engineering*, John Wiley & Sons (2007).
22. L.F. Chen, C.K. Ong, C.P. Neo, V.V. Varadan, and V. K. Varadan, *Microwave Electronics: Measurement and Materials Characterization*, Wiley (2004).
23. A. Alimenti, K. Torokhtii, E. Silva, and N. Pompeo, *Meas. Sci. Technol.* **30**, 065601 (2019).
24. N. Pompeo, R. Marcon, L. Méchin, and E. Silva, *Supercond. Sci. Technol*. **18**, 531 (2005).
25. N. Pompeo, L. Muzzi, V. Galluzzi, R. Marcon, and E. Silva, *Supercond. Sci. Technol*. **20**, 1002 (2007).
26. N. Pompeo, K. Torokhtii, A. Alimenti, A. Mancini, G. Celentano *et al*., *IEEE Trans. Appl. Supercond*. **29**, 8003405 (2019).
27. N. Pompeo, K. Torokhtii, and E. Silva, *Surface impedance measurements in thin conducting films: Substrate and finite-thickness- induced uncertainties*, *IEEE Int. Instrum. Meas. Technol. Conf.* (2017). p. 1.
28. M. Tinkham, *Introduction to Superconductivity*, 2nd Edition, McGraw-Hill, New York (1996).
29. E.B. Sonin, *Phys. Rev. B* **55**, 485 (1997).
30. N. Kopnin, *Rep. Prog. Phys*. **65**, 1633 (2002).
31. M.W. Coffey and J.R. Clem, *Phys. Rev. Lett*. **67**, 386 (1991).
32. E. Brandt, *Phys. Scr*. **T45**, 63 (1992).
33. J.I. Gittleman and B. Rosenblum, *Phys. Rev. Lett*. **16**, 734 (1966).
34. M. Golosovsky, M. Tsindlekht, and D. Davidov, *Supercond. Sci. Technol*. **9**, 1 (1996).
35. N. Kopnin and G. Volovik, *Phys. Rev. Lett.* **79**, 1377 (1997).
36. C. Caroli, P.G. De Gennes, and J. Matricon, *Phys. Lett*. **9**, 307 (1964).
37. G. Volovik, *JETP Lett*. **58**, 469 (1993).
38. A.I. Larkin, and Yu.N. Ovchinnikov, *Vortex Motion Superconductors,* in: *Nonequilibrium Supercond.* A. Langenberg, and D.N. Larkin (eds.), Elsevier, Amsterdam (1986). chap 11, p. 493.
39. G. Blatter, M. Feigel'man, V. Geshkenbein, A. Larkin, and V. Vinokur, *Rev. Mod. Phys*. **66**, 1125 (1994).
40. A. Vargunin and M.A. Silaev, *Phys. Rev. B* **96**, 214507 (2017).
41. M. Silaev and A. Vargunin, *Phys. Rev. B* **94**, 224506 (2016).
42. R. Labusch, *Phys. Status Solidi* **41**, 659 (1970).
43. I. Ghosh, L. Cohen, and J. Gallop, *Supercond. Sci. Technol.* **10**, 936 (1997).
44. J.I. Gittleman and B. Rosemblum, *J. Appl. Phys*. **39**, 2617 (1968).
45. M. Sieger, P. Pahlke, M. Lao, M. Eisterer, A. Meledin *et al*., *IEEE Trans. Appl. Supercond*. **27**, 1 (2017).
46. N. Pompeo, *J. Appl. Phys*. **117**, 103904 (2015).
47. N. Pompeo and E. Silva, *IEEE Trans. Appl. Supercond*. **28**, 8201109 (2018).
48. N. Ong and H. Wu, *Phys. Rev. B* **56**, 458 (1997).
49. E. Sonin, A. Tagantsev, and K. Traito, *Phys. Rev. B* **46**, 5830 (1992).
50. D.H. Wu, J. Booth, and S. Anlage, *Phys. Rev. Lett*. **75**, 525 (1995).
51. A.T. Dorsey, *Phys. Rev. B* **43**, 7575 (1991).
52. N. Pompeo, K. Torokhtii, and E. Silva, *Meas. Sci. Rev.* **14**, 164 (2014).
53. N. Pompeo and E. Silva, *Phys. Rev. B* **78**, 094503 (2008).
54. J. Bardeen and M. Stephen, *Phys. Rev*. **140**, 1197 (1965).
55. N. Pompeo, A. Augieri, K. Torokhtii, V. Galluzzi, G. Celentano *et al*., *Appl. Phys. Lett*. **103**, 022603 (2013).
56. J. Halbritter, *J. Supercond*. **10**, 91 (1997).
57. M. Hein, *High-Temperature-Superconductor Thin Films at Microwave Frequencies,* Berlin: Springer (1999). ISBN 978-3-540-65646-3

Фізика руху вихорів за допомогою вимірювань мікрохвильового поверхневого імпедансу
(Огляд)

N. Pompeo, A. Alimenti, K. Torokhtii, and E. Silva

Запропоновано короткий огляд результатів, отриманих при вивченні руху вихорів при високих частотах. Представлено феноменологічний баланс сил для квазіодиночних вихорів, що коливаються під впливом мікрохвильових струмів та відчувають в'язке тертя, сили пінінгу й термоактивований кріп. Обговорюються вихровий питомий опір та інші важливі вихрові параметри (в'язкість η, питомий опір у режимі регулярної течії ρ_{ff}, константа пінінгу k_p та кріп-фактор χ). Наведено приклад експериментальних результатів для ілюстрації основних аспектів розглянутих фізичних моделей.

Ключові слова: поверхневий опір, питомий опір потоку, константа пінінгу.

Физика движения вихрей посредством измерений микроволнового поверхностного импеданса (Обзор)

N. Pompeo, A. Alimenti, K. Torokhtii, and E. Silva

Предложен краткий обзор результатов, полученных при изучении движения вихрей при высоких частотах. Представлен феноменологический баланс сил для квазиодиночных вихрей, колеблющихся под воздействием микроволновых токов и испытывающих вязкое трение, силы пиннинга и термоактивированный крип. Обсуждаются вихревое удельное сопротивление и другие важные вихревые параметры (вязкость η, удельное сопротивление в режиме регулярного течения ρ_{ff}, константа пиннинга k_p и крип-фактор χ). Приведен пример экспериментальных результатов для иллюстрации основных аспектов рассматриваемых физических моделей.

Ключевые слова: поверхностное сопротивление, удельное сопротивление потока, константа пиннинга.